



Chromospheric Cannonballs on the Sun

Shuhong Yang^{1,2} , Jun Zhang^{1,2}, Xiaohong Li^{1,2} , Zhong Liu³, and Yongyuan Xiang³ ¹ CAS Key Laboratory of Solar Activity, National Astronomical Observatories, Chinese Academy of Sciences, Beijing 100101, People's Republic of China
shuhongyang@nao.cas.cn, zjun@nao.cas.cn² School of Astronomy and Space Science, University of Chinese Academy of Sciences, Beijing 100049, People's Republic of China³ Fuxian Solar Observatory, Yunnan Observatories, Chinese Academy of Sciences, Kunming 650011, People's Republic of China

Received 2019 March 13; revised 2019 May 26; accepted 2019 June 25; published 2019 July 30

Abstract

In the highly dynamic chromosphere, there exist many kinds of small-scale activities, such as spicules, surges, and Ellerman bombs. Here, we report the discovery of a new phenomenon in the chromosphere observed with the New Vacuum Solar Telescope at the Fuxian Solar Observatory. In the high tempo-spatial-resolution $H\alpha$ images, some dark or bright structures are found to fly along the curved trajectory, looking like cannonballs. Their average size, mass, and velocity are about $1.5 \times 10^9 \text{ km}^3$, $1.5 \times 10^8 \text{ kg}$, and 56 km s^{-1} , respectively. In the simultaneous (extreme-)ultraviolet images obtained by the *Solar Dynamics Observatory*, these cannonballs appear as brighter features compared to the surrounding area, implying that there exists some kind of heating during this process. The photospheric magnetograms show the magnetic flux emergence and interaction with the pre-existing fields. These observations reveal that the cannonballs are chromospheric material blobs launched due to the magnetic reconnection between emerging magnetic flux and the pre-existing loops.

Key words: magnetic reconnection – Sun: activity – Sun: chromosphere – Sun: magnetic fields

Supporting material: animations

1. Introduction

The solar chromosphere is the necessary layer of energy transport from the photosphere to the corona. Consequently, the chromosphere of the Sun plays an important role in coronal heating and solar wind acceleration. As the temperature minimum layer of the solar atmosphere, the chromosphere has been extensively imaged in the $H\alpha$ wavelength with ground-based and space-based instruments for many years. Dark fibrils are ubiquitous in the solar chromosphere, and they are filled with cool and dense material (Aschwanden et al. 2016). Comparing the fibrils in the $H\alpha$ images with the extrapolated potential fields from the photospheric magnetograms, the chromospheric magnetic fields are found to be significantly nonpotential (Woodard & Chae 1999). The free energy stored in nonpotential fields can be released into power plentiful solar activities in the chromosphere (Moore et al. 2010; Sterling et al. 2015; Yang et al. 2015; Ni et al. 2016; Xue et al. 2016; Yang & Xiang 2016). Spicules, appearing as thin and dynamic extrusions if observed at the solar limb, are ubiquitous in the chromosphere (Sterling 2000; De Pontieu et al. 2004). De Pontieu et al. (2007) found that some spicules are driven by shock waves along magnetic field lines, and some that send material through the chromosphere at higher speeds are caused by magnetic reconnection. Surges, jet-like structures observed in the $H\alpha$ wavelength, are always associated with magnetic flux emergence or cancellation in observations, and are theoretically deemed to result from magnetic reconnection (Yokoyama & Shibata 1995; Chae et al. 1999; Shibata et al. 2007). Ellerman bombs are small-scale short-lived brightenings in both wings of the $H\alpha$ line (Ellerman 1917; Fang et al. 2006; Tian et al. 2016). Their triggering mechanism is suggested to

be a reconnection process caused by the low-lying magnetic fields in the chromosphere (Georgoulis et al. 2002; Reid et al. 2016). Magnetohydrodynamic (MHD) simulations also show that, when the emerging magnetic flux expands in the atmosphere, magnetic reconnection takes place and consequently heats the local dense plasma (Isobe et al. 2007; Archontis & Hood 2009).

With the improvement of observational instrument, it is a good opportunity for us to further study the fine-scale chromospheric structures. In this Letter, we report the discovery of a new phenomenon in the chromosphere, i.e., flying cannonball-like structures (hereafter cannonballs), based on the high tempo-spatial-resolution $H\alpha$ observations from the New Vacuum Solar Telescope (NVST; Liu et al. 2014) of China.

2. Observations and Data Analysis

With a clear aperture of 985 mm, the NVST is the primary facility of the Fuxian Solar Observatory operated by Yunnan Observatories. The $H\alpha$ channel is used to image the highly dynamic solar chromosphere at high tempo-spatial resolution. The $H\alpha$ filter is a tunable Lyot filter with a bandwidth of 0.25 \AA , which can scan spectra in the $\pm 5 \text{ \AA}$ range with a step size of 0.1 \AA . The present study is mainly based on three events with the $H\alpha$ line-center (6562.8 \AA) observations, i.e., 2017 October 28 05:43–08:01 UT, 2017 August 06 08:00–10:06 UT, and 2018 May 11 00:50–05:02 UT. Their time cadences are 29 s, 31 s, and 9 s, respectively. The fields of view (FOVs) are $126'' \times 126''$ with the pixel size of $0''.136$. The Level 0 data are first calibrated to Level 1, including dark current subtraction and flat field correction. Then the calibrated Level 1 images are reconstructed to Level 1+ by speckle masking (Weigelt 1977; Lohmann et al. 1983).

The simultaneous line of sight (LOS) magnetograms from the Helioseismic and Magnetic Imager (HMI; Scherrer et al. 2012)



Original content from this work may be used under the terms of the [Creative Commons Attribution 3.0 licence](https://creativecommons.org/licenses/by/3.0/). Any further distribution of this work must maintain attribution to the author(s) and the title of the work, journal citation and DOI.

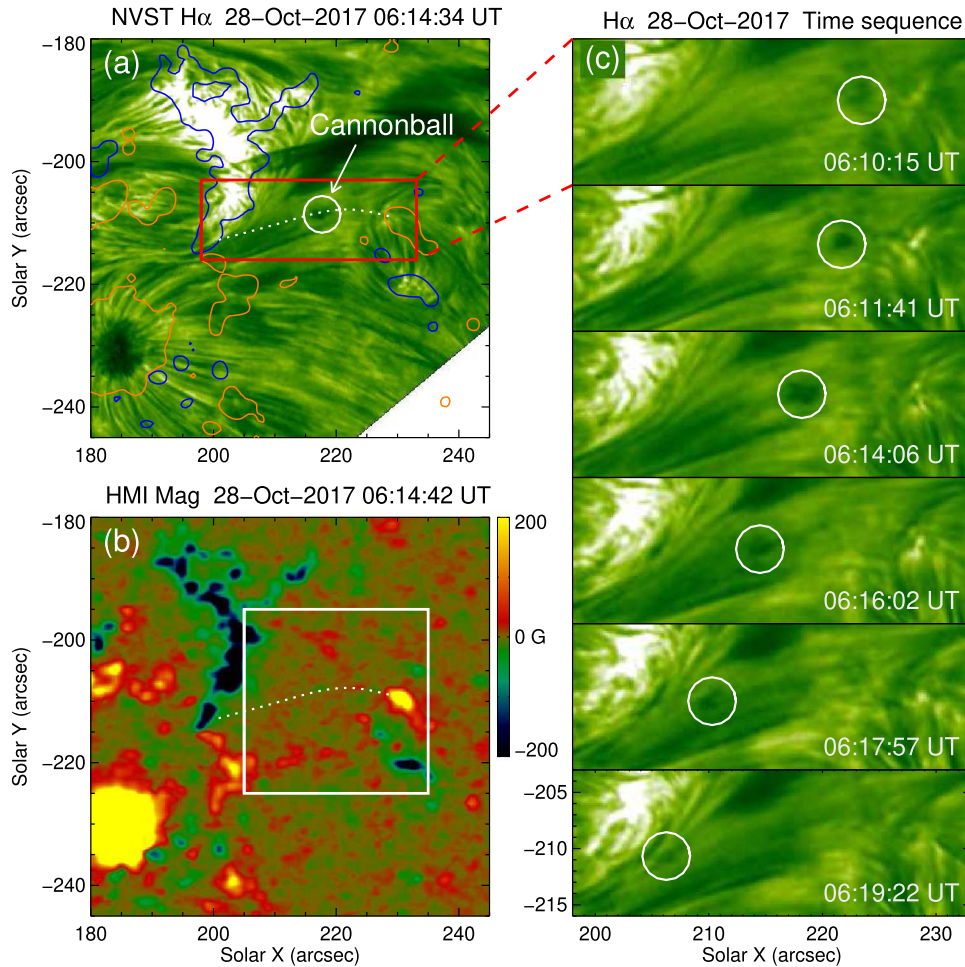


Figure 1. Panels (a)–(b): NVST H α image and HMI LOS magnetogram displaying the chromospheric cannonball-like structure and the underlying photospheric magnetic environment, respectively. Panel (c): time sequence of H α images showing the movement of the cannonball along a curved trajectory. The brown and blue solid curves in panel (a) are the contours of the photospheric magnetic fields at +30 G and -30 G, respectively. The white circles and dotted curves outline the cannonball and its flying trajectory, respectively. The square in panel (b) denotes the FOV of Figures 2(a)–(c). An animation of the NVST H α images is available in the online Journal. The unannotated animation corresponds to the same physical scale as Panel (a), and runs from 06:02 to 06:26 UT.

(An animation of this figure is available.)

and the multi-wavelength images from the Atmospheric Imaging Assembly (AIA; Lemen et al. 2012) on board the *Solar Dynamics Observatory* (SDO; Pesnell et al. 2012) are also used. The HMI LOS magnetograms have a cadence of 45 s and a spatial sampling of $0''.5 \text{ pixel}^{-1}$, and the AIA (extreme-)ultraviolet (EUV/UV) full-disk images have a cadence of 12/24 s and a pixel size of $0''.6$. Here, we mainly present the AIA observations in 304 Å (UV) and 171 Å (EUV) lines, in which the cannonballs have the conspicuous counterparts. All the HMI and AIA data are calibrated to Level 1.5 with the standard routine under the Solar Software package. Then the data on October 28 and August 6 are de-rotated differentially to the reference times of 06:00 UT and 08:46 UT, respectively. The NVST H α images are coaligned with the SDO data using the cross-correlation method according to specific features.

3. Results

The FOV of the NVST H α observations on 2017 October 28 is centered at $(190'', -200'')$. Figure 1(a) displays the appearance of a sub-FOV H α image at 06:14:34 UT, where a cannonball is enclosed by the white circle. The dotted curve delineates the trajectory, along which the cannonball moved

from the west to the east. The origination and landing sites of the cannonball correspond to the positive and negative magnetic patches, respectively (panel (b)). To see the movement well, we show a sequence of enlarged H α images in Figure 1(c), and the cannonball at each time is outlined by a white circle. At 06:10:15 UT, the cannonball can be well identified as a dark structure. One and a half minutes later, the cannonball was more conspicuous and moved to a new site to the east (see the online animated Figure 1(a)). In the following seven and a half minutes, the cannonball went on flying with the average velocity of about 23.4 km s^{-1} .

Because the cannonball appears as a quasi-circular feature in the H α images, it can be assumed to be a ball in three dimensions. If the diameter of a ball measured in the observational image is D , then the size (i.e., volume) V is $4/3 \times \pi \times (D/2)^3$. In the 2017 October 28 event, the D of the cannonball is 1270 km, so the size of the cannonball is $1.07 \times 10^9 \text{ km}^3$. The density of the cannonball is considered to be $1 \times 10^{-10} \text{ kg m}^{-3}$, i.e., the density of the chromosphere (Beckers 1968). Thus the cannonball has the mass of $1.07 \times 10^8 \text{ kg}$.

In order to study the temperature character of the cannonball, we examine the multi-wavelength images and corresponding online animation in Figures 2(a)–(c). We find that, for the dark

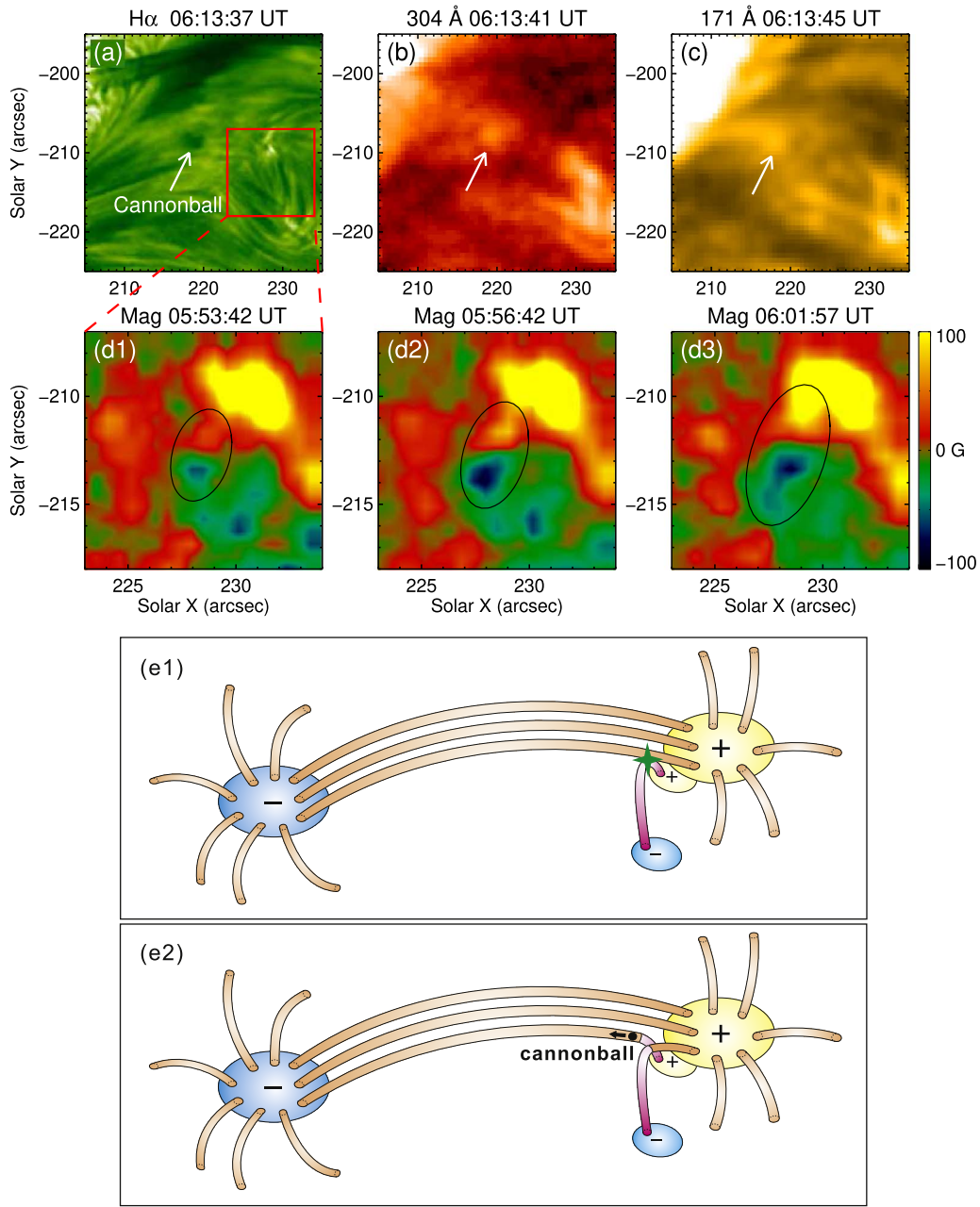


Figure 2. Panels (a)–(c): NVST $H\alpha$, AIA 304, and 171 Å images displaying the different appearance of the cannonball (denoted by the arrows). Panels (d1)–(d3): HMI LOS magnetograms showing the emergence of a bipole (outlined by the ellipses) at the origination site of the cannonball. Panels (e1)–(e2): schematic drawings illustrating the magnetic reconnection resulting in the formation of cannonballs. Animations of panels (a)–(c) and (d1)–(d3) are available in the online Journal. The animation of the NVST $H\alpha$, AIA 304, and 171 Å images runs from 06:10 to 06:18 UT, while the animation of the HMI LOS magnetogram runs from 05:51 to 06:11 UT. Neither animation is annotated.

(Animations (a and b) of this figure are available.)

cannonball in the $H\alpha$ image (denoted by the arrow in Figure 2(a)), there are clear bright counterparts in 304 Å (panel (b)) and 171 Å (panel (c)) images. In the UV (304 Å) and EUV (171 Å) lines, the emission of these counterparts is significantly higher than the surrounding area. Because magnetic field evolution always plays a crucial role in solar active events, we also examine the photospheric magnetograms at the origination site of the cannonball. A time sequence of HMI magnetograms during a 15 minute period before the cannonball onset is shown in the middle panels of Figure 2(d) and corresponding online animation. The positive polarity appears as the red–yellow

patches, and the negative polarity as the green–blue ones. At 05:53 UT, a faint bipole (outlined by the ellipse in panel (d1)) began to emerge at the southeast location of the pre-existing positive magnetic field. Three minutes later, the bipole grew much larger (see panel (d2)). Meanwhile, the bipolar patches with opposite polarities separated from each other, and the positive patch moved to and merged with the pre-existing positive field (panel (d3)).

Different from the above event, the NVST $H\alpha$ images on 2017 August 6 present a bright cannonball instead of a dark one. Figure 3(a) shows the overview of the $H\alpha$ image where

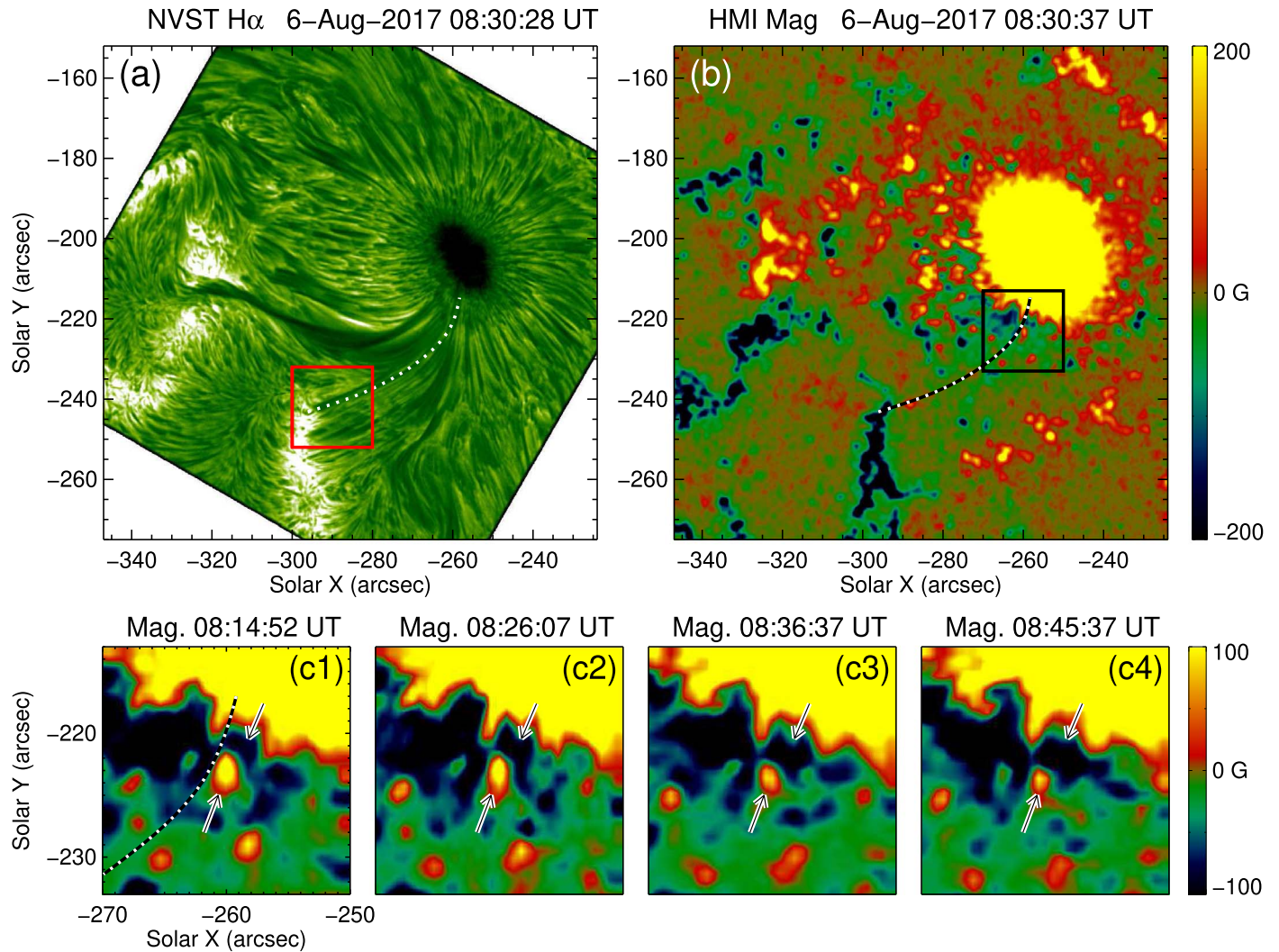


Figure 3. Panels (a)–(b): overview of the $H\alpha$ observation and the photospheric magnetic field, respectively. The dotted curves delineate the fibril along which the cannonball flew. The box in panel (b) outlines the FOV of panels (c1)–(c4), and the box in panel (a) outlines the FOV of Figure 4. Panels (c1)–(c4): sequence of HMI magnetograms showing the magnetic field evolution at the initiation site of the cannonball. The upper arrows indicate the emerging negative field and the lower arrows denote the disappearing positive field. An animation of the HMI magnetograms in panels (c1)–(c4) is available in the online Journal. The HMI magnetogram animation runs from 08:07 to 08:45 UT and is not annotated.

(An animation of this figure is available.)

there are many long fibrils extending from the sunspot to the remote region. The dotted curve delineates a fibril along which the cannonball moved. In the HMI photospheric magnetogram (panel (b)), the trajectory of the cannonball is also overlaid. The cannonball originated from the penumbral positive field and flew to the southeast enhanced negative field. The magnetic field evolution at the origination site of the cannonball is outlined by the black square in panel (b) and displayed in panels (c1)–(c4). We can see that the negative polarity patch pointed by the upper arrows continued growing, while the positive polarity patch denoted by the lower arrows shrank significantly (see the animated HMI magnetogram in the online Figure 3). These changes indicate the existence of magnetic emergence and cancellation at the origination site of the cannonball.

In the $H\alpha$ images in Figure 4, the cannonball can be directly identified (top panels; see the online $H\alpha$ animation). The cannonball outlined by the red circles moved from upper right to the lower left. The size of the cannonball is about $1.74 \times 10^9 \text{ km}^3$, and the mass is estimated to be $1.74 \times 10^8 \text{ kg}$. As the cannonball is somewhat faint in the Level 1+ data, we use

the $H\alpha$ running difference images to show it (panels (b1)–(b4)). We can see that the cannonball is more conspicuous in the running difference images, where a bright feature followed by an adjacent dark one represents the cannonball. Its average movement velocity is about 50.0 km s^{-1} . In addition, we check the multi-wavelength images to study the counterpart of the cannonball. The bright chromospheric cannonball in the $H\alpha$ image (panel (c)) also appears as a bright feature in both AIA 304 Å (panel (d)) and 171 Å (panel (e)) images (and the online animation of these Figure 4 panels). Particularly, in the 304 Å images, the cannonball’s brightness relative to the surrounding area is more prominent, compared with its appearance in the 171 Å images.

Figure 5(a) shows the overview of the $H\alpha$ image on 2018 May 11, when two bright cannonballs were observed (see the online animation of the $H\alpha$ images in Figure 5). The cannonballs flew to the northwest along the dotted curve in panel (b). Because the signals of the cannonballs are weak in the $H\alpha$ Level 1+ images, we study them in the running difference images (see panels (c1)–(c4)), where a bright feature

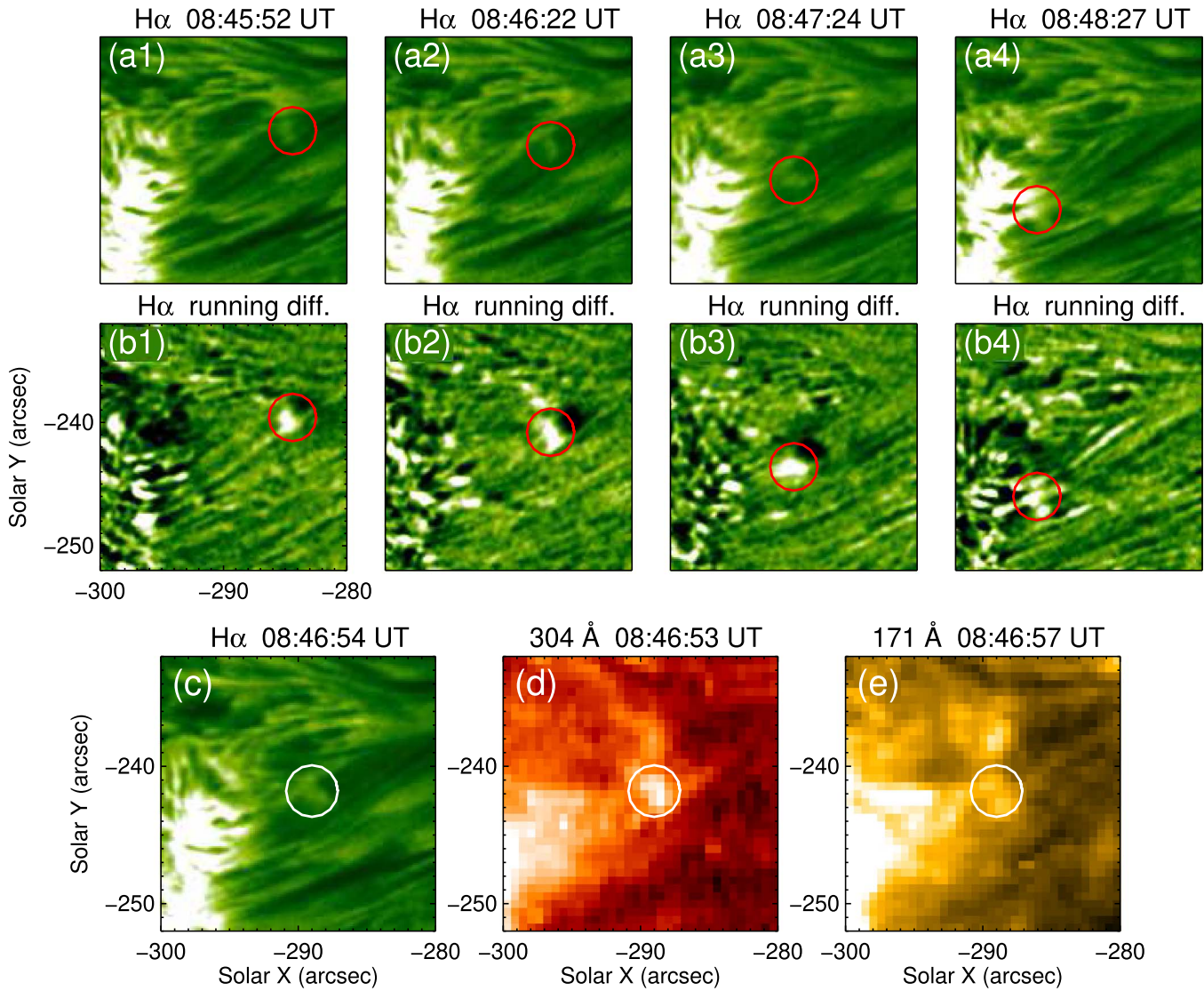


Figure 4. Panels (a1)–(a4): $H\alpha$ Level 1+ images displaying the flying cannonball (outlined by the circles). Panels (b1)–(b4): $H\alpha$ running difference images corresponding to the upper panels. Panels (c)–(e): multi-wavelength appearance of the cannonball in $H\alpha$, 304 Å, and 171 Å, respectively. An animation of the $H\alpha$ Level 1+ and the $H\alpha$ running difference images is available in the online Journal. The $H\alpha$ animation runs from 08:31 to 08:51 UT. A second animation of the multi-wavelength appearance of the cannonball is available and runs from 08:44 to 08:49 UT. Neither animation is annotated.

(Animations (a and b) of this figure are available.)

followed by an adjacent dark one represents a cannonball. These two cannonballs (outlined by the white and red circles, respectively) originated side by side from the southeast end of the dark fibrils (see panel (c1)). The left cannonball flew to the northwest with a mean velocity of 60 km s^{-1} , and the right one was much faster with the average velocity of 90 km s^{-1} . Their average size and mass are $1.65 \times 10^9 \text{ km}^3$ and $1.65 \times 10^8 \text{ kg}$, respectively. When we check the underlying magnetograms, we find that the cannonballs were launched from the intranetwork magnetic field with mixed polarities and flew to the network field with negative field. The emergence and cancellation of small-scale intranetwork fields are widespread, which can contribute to the formation and launch of cannonballs.

4. Conclusions and Discussion

Based on the $H\alpha$ observations from the NVST, we find a new phenomenon in the highly dynamic chromosphere. Some dark or bright structures flew along the curved trajectory,

looking like cannonballs. The average size, mass, and velocity of the cannonballs are about $1.53 \times 10^9 \text{ km}^3$, $1.53 \times 10^8 \text{ kg}$, and 55.9 km s^{-1} , respectively. In the simultaneous UV and EUV images from the AIA, these cannonballs appear as brighter structures compared to the surrounding environment. The photospheric magnetograms from the HMI show the emergence of magnetic flux and the consequent interaction with the pre-existing flux.

The reasons why we call these observed structures cannonballs are as follows. (1) They have similar morphology to cannonballs because they appear as quasi-spherical blobs in observations. (2) Their movement consists of a rising stage and then a falling stage in height, as they originate from one end of the curved field lines and move toward the other end, which is also the general behavior of flying cannonballs.

To illustrate the cannonball formation, we propose a cartoon as shown in Figures 2(e1)–(e2). Initially, there exists a positive patch connected with remote negative field by large-scale loops

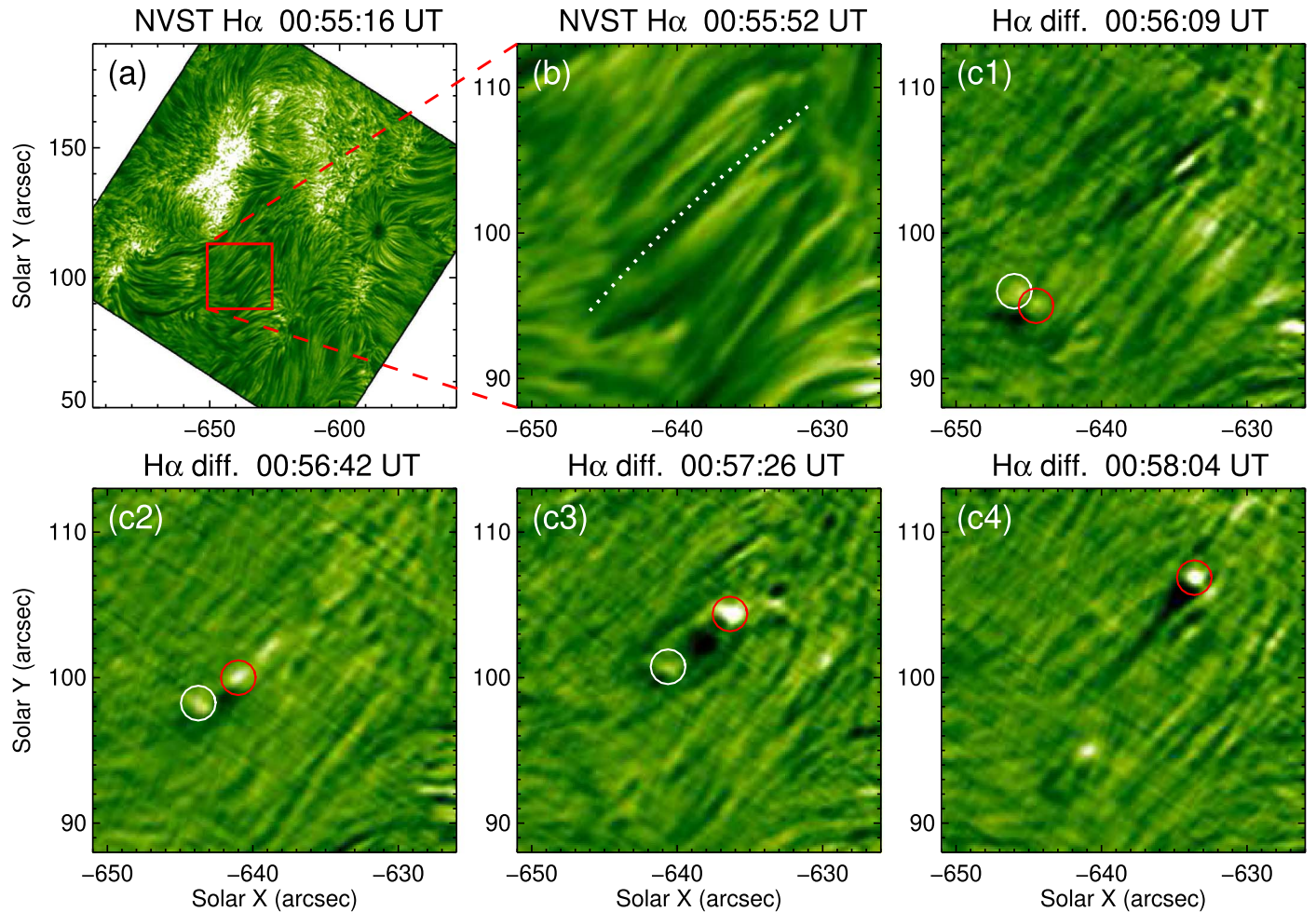


Figure 5. Panel (a): overview of the $H\alpha$ observation on 2018 May 11. Panel (b): $H\alpha$ Level 1+ image of a sub-FOV where the dotted curve delineates the trajectory of two cannonballs. Panels (c1)–(c4): $H\alpha$ running difference images showing the movement of two cannonballs outlined with the white and red circles, respectively. An animation of the $H\alpha$ Level 1+ and the $H\alpha$ running difference sub-FOV images is available in the online Journal. The animation is not annotated and runs from 00:55:16 to 00:58:28 UT.

(An animation of this figure is available.)

(panel (e1)). A bipole emerges at the adjacency to the pre-existing positive patch, and its two opposite polarities are connected by small-scale loops. As the emerging bipolar patches separate, the small-scale loops rise toward the overlying loops. Eventually, the newly emerged small-scale loops meet and reconnect with the overlying large-scale field lines. Due to the reconnection, the chromospheric material is expelled from the reconnection site and flies along the large-scale loops, forming a cannonball (panel (e2)).

In the observations, both the dark and bright cannonballs have similar behaviors. For these $H\alpha$ cannonballs, there are prominent bright counterparts in the UV/EUV lines, implying the existence of some kind of heating mechanism. We suggest that magnetic reconnection may result in the heating of the cannonballs as observed. Previous studies have shown that magnetic flux emergence and cancellation are often associated with magnetic reconnection (Zhang et al. 2001; Yang et al. 2011; Hansteen et al. 2017). As shown in Figures 2 and 3, we indeed observed the magnetic emergence/cancellation in the photosphere at the origination sites. For the 2018 May 11 event, the initiation site of the cannonballs is located in the intranetwork region, where magnetic reconnection between emerging flux with mixed polarities is ubiquitous. When magnetic reconnection takes

place, magnetic energy is converted into thermal energy and kinetic energy (Zweibel & Yamada 2009; Cirtain et al. 2013; Wyper et al. 2017). Therefore, the cannonballs can be consequently launched and heated. However, for the heating of the cannonballs, another possibility could not be excluded, i.e., being heated by the shock front of the flying cannonballs. The flying cannonballs can play an importance role in transferring material and energy in the solar atmosphere.

We should note that reconnection physics under solar conditions has not been understood well enough to state the thermal physics with any certainty. Magnetic reconnection is a rapid, dynamic change in topology leading to bulk flows, but the temperature of the gas is highly uncertain. In the solar chromosphere it may be simpler than in the corona, considering that the reconnecting Lorentz forces act only on ions and that the chromosphere is almost fully neutral, which will lead to ion-neutral heating. However, this is just one aspect of magnetic reconnection under chromospheric conditions.

The highly dynamic structures (such as fast-moving bright blobs) in the chromosphere were also revealed in the Swedish 1 m Solar Telescope (SST) observations (van Noort & Rouppe van der Voort 2006). However, the cannonballs are different from those previous observed structures. The SST observed the

bright blobs, while the NVST observed both the dark and bright features. The SST bright blobs are high-velocity (up to 240 km s^{-1}) structures, while the NVST cannonballs are low-velocity features with the average velocity of about 37 km s^{-1} . For the SST blobs, there appear many conspicuous brightenings at the origination sites, which cannot be identified during the initiation of the NVST cannonballs. Moreover, there are significant topological changes in the SST observations, while the chromospheric structures observed with the NVST are generally quiet and stable. Therefore, the SST blobs are associated with eruptive events, and the NVST cannonballs only result from small-scale magnetic activity in the chromosphere.

As described in the previous studies (e.g., Schrijver 2001; Antolin et al. 2010; Antolin & Rouppe van der Voort 2012), when the coronal matter cools down catastrophically due to the thermal instability, the condensations fall from coronal heights along coronal loops to the footpoints under the action of the solar gravity, forming “coronal rain.” While in our observations, especially clearly displayed in Figures 1 and 5, cannonballs are chromospheric material that originated at one end of the magnetic loops and flew to the other end. Therefore, the cannonballs we observed are different from frequently studied coronal rain.



Both the cannonballs and type II spicules are thought to be the consequences of magnetic reconnection, which can be used to interpret the fact that they have the similar speeds. However, they are different phenomena, not merely because the cannonballs occur along locally closed field lines instead of open ones. As revealed by the previous studies (e.g., De Pontieu et al. 2007; Pereira et al. 2012), type II spicules are thin jet-like features (no more than 200 km in width and at least several Mm in length). The cannonballs shown in this Letter are quasi-spherical, and much wider and shorter than type II spicules. From these three events studied here, we expect to find about 40 cannonballs on the Sun at any given time. This number is much lower than that of type II spicules, which is surmised to be several tens per supergranule (e.g., Moore et al. 2011; Sekse et al. 2012).

An interesting question is therefore raised: why are the cannonballs like “blobs” of fluid instead of “jets” that are commonly thought to be type II spicules? The cannonballs appear much more morphologically like the coronal rain than jets. How can this be? We hope that the answer can be given in the near future through further studies.

We are grateful to the referee for the constructive comments and valuable suggestions. The data are used courtesy of NVST, HMI, and AIA science teams. This work is supported by the National Natural Science Foundations of China (11673035, 11790304, 11533008, 11790300), Key Programs of the

Chinese Academy of Sciences (QYZDJ-SSW-SLH050), and the Youth Innovation Promotion Association of CAS (2014043).

ORCID iDs

Shuhong Yang  <https://orcid.org/0000-0002-6565-3251>
 Xiaohong Li  <https://orcid.org/0000-0001-8164-5633>
 Yongyuan Xiang  <https://orcid.org/0000-0002-5261-6523>

References

- Antolin, P., & Rouppe van der Voort, L. 2012, *ApJ*, 745, 152
 Antolin, P., Shibata, K., & Vissers, G. 2010, *ApJ*, 716, 154
 Archontis, V., & Hood, A. W. 2009, *A&A*, 508, 1469
 Aschwanden, M. J., Reardon, K., & Jess, D. B. 2016, *ApJ*, 826, 61
 Beckers, J. M. 1968, *SoPh*, 3, 367
 Chae, J., Qiu, J., Wang, H., & Goode, P. R. 1999, *ApJL*, 513, L75
 Cirtain, J. W., Golub, L., Winebarger, A. R., et al. 2013, *Natur*, 493, 501
 De Pontieu, B., Erdélyi, R., & James, S. P. 2004, *Natur*, 430, 536
 De Pontieu, B., McIntosh, S., Hansteen, V. H., et al. 2007, *PASJ*, 59, S655
 Ellerman, F. 1917, *ApJ*, 46, 298
 Fang, C., Tang, Y. H., Xu, Z., Ding, M. D., & Chen, P. F. 2006, *ApJ*, 643, 1325
 Georgoulis, M. K., Rust, D. M., Bernasconi, P. N., & Schmieder, B. 2002, *ApJ*, 575, 506
 Hansteen, V. H., Archontis, V., Pereira, T. M. D., et al. 2017, *ApJ*, 839, 22
 Isobe, H., Tripathi, D., & Archontis, V. 2007, *ApJL*, 657, L53
 Lemen, J. R., Title, A. M., Akin, D. J., et al. 2012, *SoPh*, 275, 17
 Liu, Z., Xu, J., Gu, B.-Z., et al. 2014, *RAA*, 14, 705
 Lohmann, A. W., Weigelt, G., & Wirmitzer, B. 1983, *ApOpt*, 22, 4028
 Moore, R. L., Cirtain, J. W., Sterling, A. C., & Falconer, D. A. 2010, *ApJ*, 720, 757
 Moore, R. L., Sterling, A. C., Cirtain, J. W., & Falconer, D. A. 2011, *ApJL*, 731, L18
 Ni, L., Lin, J., Roussev, I. I., & Schmieder, B. 2016, *ApJ*, 832, 195
 Pereira, T. M. D., De Pontieu, B., & Carlsson, M. 2012, *ApJ*, 759, 18
 Pesnell, W. D., Thompson, B. J., & Chamberlin, P. C. 2012, *SoPh*, 275, 3
 Reid, A., Mathioudakis, M., Doyle, J. G., et al. 2016, *ApJ*, 823, 110
 Scherrer, P. H., Schou, J., Bush, R. I., et al. 2012, *SoPh*, 275, 207
 Schrijver, C. J. 2001, *SoPh*, 198, 325
 Sekse, D. H., Rouppe van der Voort, L., & De Pontieu, B. 2012, *ApJ*, 752, 108
 Shibata, K., Nakamura, T., Matsumoto, T., et al. 2007, *Sci*, 318, 1591
 Sterling, A. C. 2000, *SoPh*, 196, 79
 Sterling, A. C., Moore, R. L., Falconer, D. A., & Adams, M. 2015, *Natur*, 523, 437
 Tian, H., Xu, Z., He, J., & Madsen, C. 2016, *ApJ*, 824, 96
 van Noort, M. J., & Rouppe van der Voort, L. H. M. 2006, *ApJL*, 648, L67
 Weigelt, G. P. 1977, *OptCo*, 21, 55
 Woodard, M. F., & Chae, J. 1999, *SoPh*, 184, 239
 Wyper, P. F., Antiochos, S. K., & DeVore, C. R. 2017, *Natur*, 544, 452
 Xue, Z., Yan, X., Cheng, X., et al. 2016, *NatCo*, 7, 11837
 Yang, S., & Xiang, Y. 2016, *ApJL*, 819, L24
 Yang, S., Zhang, J., Li, T., & Liu, Y. 2011, *ApJL*, 732, L7
 Yang, S., Zhang, J., & Xiang, Y. 2015, *ApJL*, 798, L11
 Yokoyama, T., & Shibata, K. 1995, *Natur*, 375, 42
 Zhang, J., Wang, J., Deng, Y., & Wu, D. 2001, *ApJL*, 548, L99
 Zweibel, E. G., & Yamada, M. 2009, *ARA&A*, 47, 291